Simulation and Analysis of Current Ripple in an Experimental DC Nanogrid

João Paulo de Andrade Machado[1], Victor Parente de Oliveira Alves[1], Arthur Correa da Fonseca[1], Wilson Negrão Macêdo[1], and Marcos André Barros Galhardo[1]

[1] Grupo de Estudos e Desenvolvimento de Alternativas Energéticas/UFPA, Belém (Brazil)

Abstract

The global challenges of climate change and growing energy demand have accelerated the adoption of renewable energy systems, particularly for remote communities lacking access to conventional power grids. Direct Current Distribution Nanogrids (DCDNs) offer an efficient solution for integrating renewables, but they can face power quality challenges due to the inverters required for AC loads. This study presents an analysis of current ripple phenomena within a DCDN, modeled in MATLAB/SIMULINK and based on an experimental system designed to supply power to remote communities in the Amazon. The system comprises three distributed photovoltaic generators with integrated storage units, supplying power to three distinct load banks, one of which includes an inverter for AC appliances. Through five simulations with progressively increasing power demands on the AC load, the propagation and impact of ripple were investigated throughout the grid. The inverter is the primary source of ripple, introducing significant harmonic distortions with a fundamental frequency of 120 Hz on the DC side. A correlation was established between higher ripple magnitudes, increased circulation of non-active power, and consequently, greater power losses in the distribution grid. The ripple factor (RF) was used as a metric for quantifying these disturbances and their impact on system efficiency. These findings are important for designing robust off-grid DC power systems, highlighting the need to mitigate ripple effects to ensure power quality and reliability.

Keywords: nanogrid, direct current, electronic device modeling, simulation, communities

1. Introduction

A DCDN is a microgrid on a small scale and has emerged as a prominent configuration for electrical distribution. These systems have gained importance due to their greater efficiency in integrating renewable sources, loads, and storage systems. This integration is increasingly common in residential and commercial buildings, where photovoltaic systems, battery energy storage systems, electric vehicles, and electronic loads are used (Machado et al., 2023). As a result, it facilitates the use of DC electricity distribution and can eliminate the need for DC/AC conversion stages.

Consequently, this configuration proves to be advantageous technically as most DCDN deployments aim to reduce conversion costs and increase overall efficiency. However, some loads are not adapted to work directly in DC and still need an inverter to operate correctly.

In the context of small demands in remote locations, the application of DCDN is also promising and can face power quality challenges related to current ripples in the DC grid due to an inverter. Therefore, studies on this event are crucial for improving the quality, reliability, and efficiency of the electrical energy system (da Fonseca et al., 2025; Fuchs et al., 2024; Ma et al., 2023).

This study aims to analyze the current ripples and their effects due to the operation of an inverter in an open structure DCDN with passive operation mode, focusing on modeling, simulation, and evaluating its operational performance. The system model is based on a real DCDN installed in the test area of the building of the Grupo de Estudos e Desenvolvimento de Alternativas Energéticas at Universidade Federal do Pará (GEDAE/UFPA), located in the city of Belém, Pará, Brazil (this structure and design can be replicated for electricity supply in remote locations). Although a full-scale physical system is available for testing and measurements, simulations play a role in the understanding of system behavior, enabling controlled experimentation and supporting

10.18086/swc.2025.07.13 Available at http://proceedings.ises.org

predictive analysis under various operating conditions.

2. DC Nanogrid

Figure 1, Figure 2 and Figure 3 show the model of the nanogrid components simulated in Simulink/Matlab, the DCDN modeled and the real DCDN installed and the connection diagram of the grid, respectively.

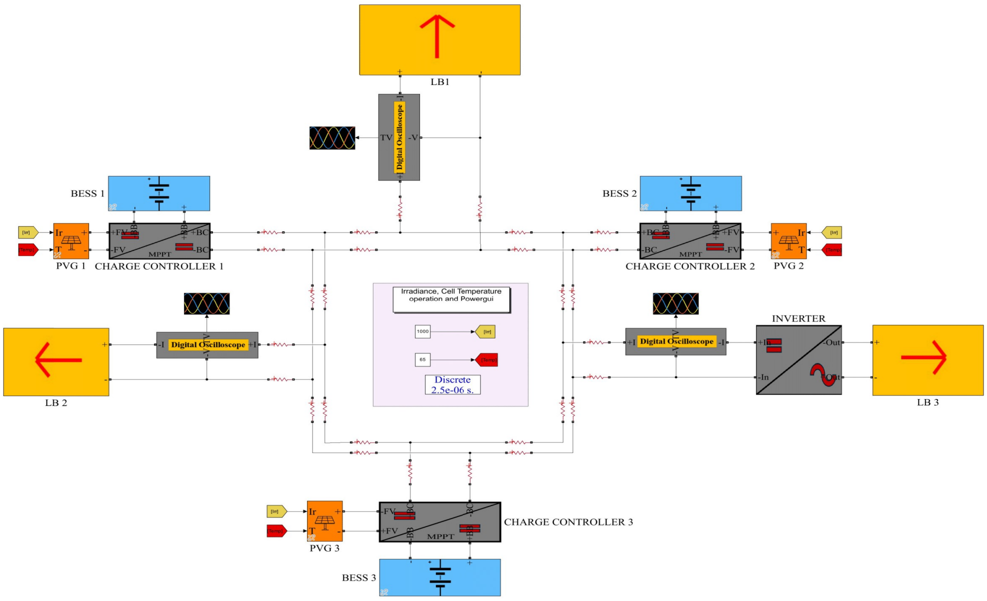

Figure 1: Nanogrid model simulated in MATLAB/Simulink.

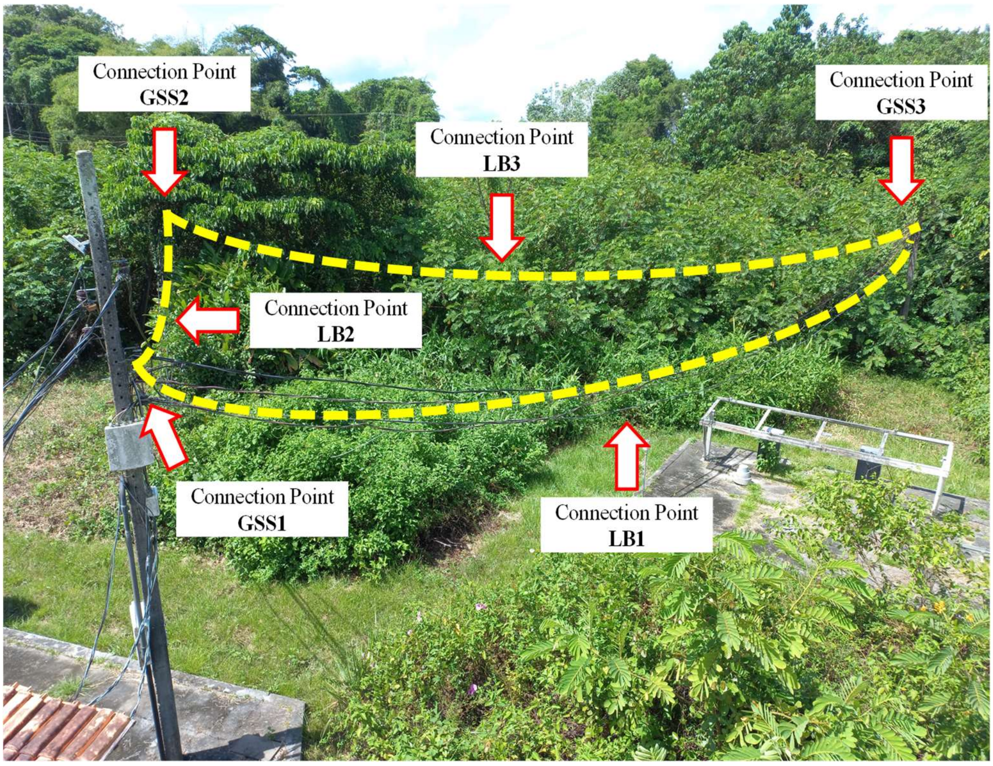

Figure 2: DCDN installed in GEDAE's laboratory area.

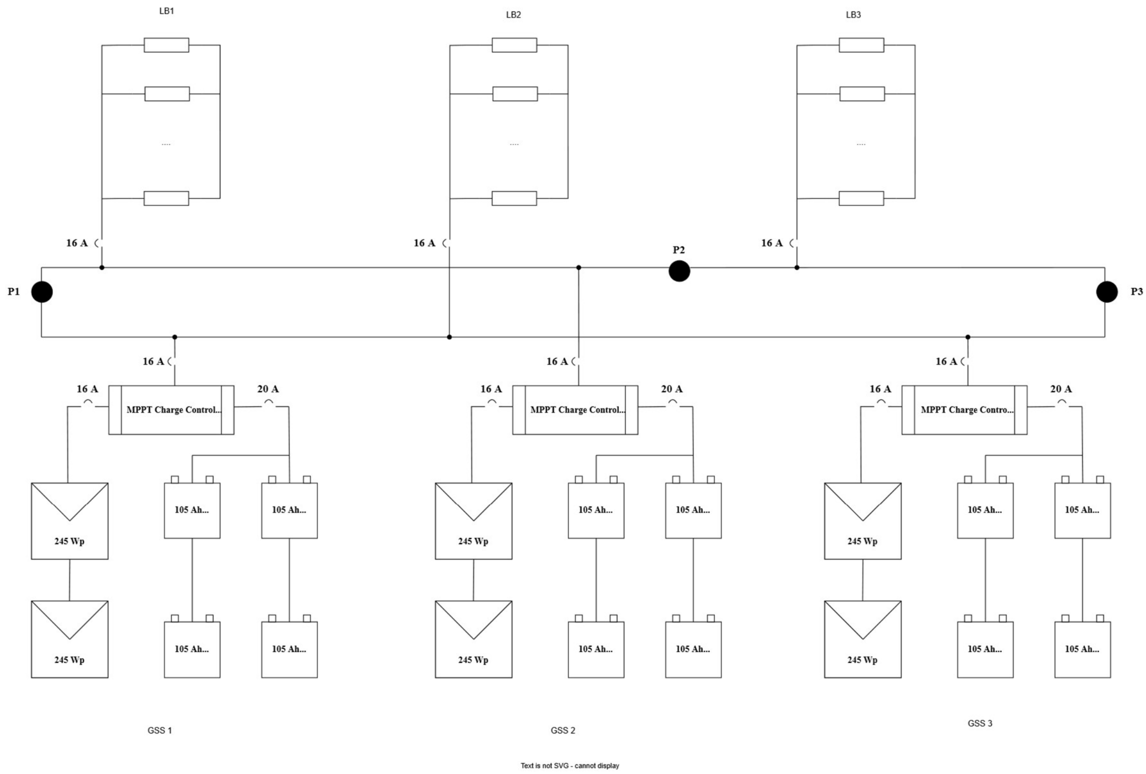

Figure 3: DCDN connections diagram.

The modeling of the experimental DCDN was based on previous works developed by Machado et al., 2023. It is composed of 3 Generation and Storage Systems (GSS), 3 load banks, and grid cables connecting these devices. Each GSS consists of its respective Photovoltaic Generator (PVG) and Battery Energy Storage System (BESS). The PVG is formed by the series association of two multicrystalline solar modules with 245 Wp. Also, the BSS consists of 4 stationary lead-acid solar batteries, which have a nominal voltage of 24 V and a capacity of 200 Ah. A charge controller with Maximum Power Point Tracking (MPPT) and three-stage charging algorithm connects the GSS's elements and by its outputs permits their access to the distribution grid at different connection points.

Each load bank model considers the types of loads that can be used in DC distribution systems. The LB1 is a resistive load capable of dissipating a power up to 162 W for a voltage of 24 V. LB2 is composed of LED lighting with a DC-DC converter, considering a total power of 50 W. Finally, the LB3 uses an off-grid inverter to interface the DC grid with AC nonlinear loads that consist of a 60 W TV and different LED lamps. So, the demand varies from 87 W to 358 W. The inverter model consists of a push-pull converter in series with an H-bridge with PI control. The inverter's rms voltage and frequency output are 127 V and 60 Hz, respectively.

2.1. PV Array

The installed DCDN's PV arrays consist of two Yingli YL-245P-29B multicrystalline silicon modules connected in series. The system PV arrays were modeled by Machado et al. (2023), using the five-parameter PV array block from Simulink's Simscape library. Model validation involved comparing simulated I-V and P-V curves with those obtained from a module test conducted using the Highlight 3c solar simulator by PASAN MEASUREMENT SYSTEMS at GEDAE's laboratory. To evaluate the model's accuracy, the Standard Deviation of the Percent Error (SDPE) was used to evaluate the model's accuracy showing values of 1.84 for the I-V curve and 2.98 for the P-V curve. These results indicate that the simulated data closely match the real measurements.

The PV generators and their Simulink representation are shown in Figure 4.

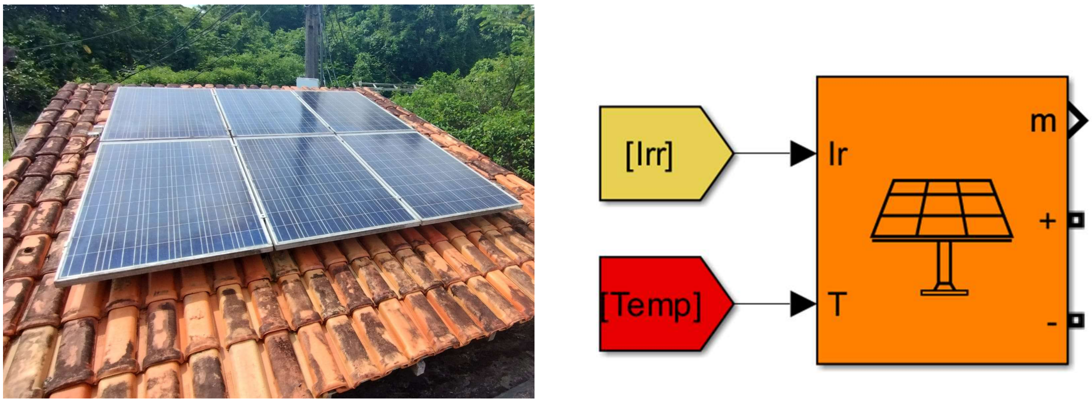

Figure 4: PV generators and their Simulink block.

2.2. MPPT Charge Controller

The MPPT Charge Controller model was based on the work of Tan, Er, et al. (2020) which consists of a buck converter and an MPPT algorithm associated with a charge control (Figure 5). The block Charge Controller is responsible for employing the MPPT algorithm and implementing the three-stage battery charging (bulk, absorption, float). By this block, it is possible to define the Absorption Voltage, which is defined for these BSS to 28.8 V. Some modifications were introduced to the Solar Charge Control (Machado et al., 2023; Tan, Er, et al., 2020).

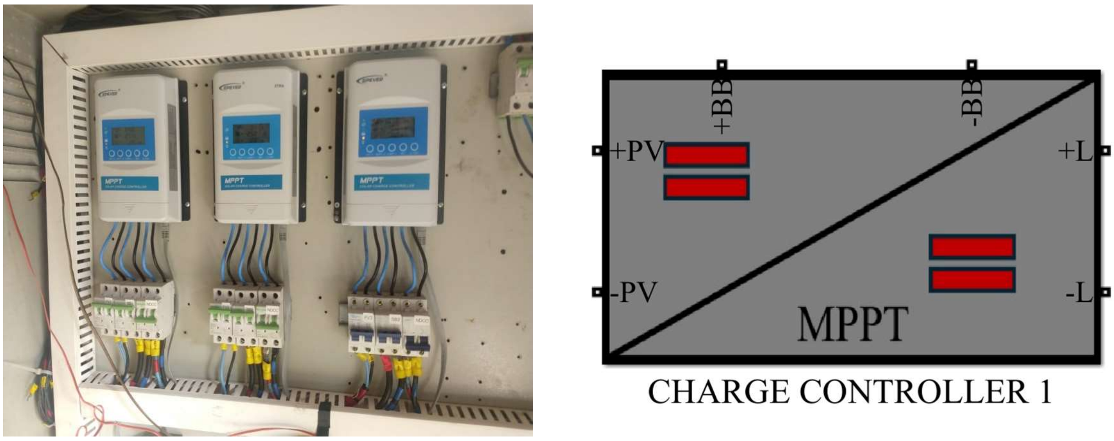

Figure 5: Charge controllers and their Simulink block.

2.3. Battery Storage System

The storage system of the DCDN is formed by 4 MOURA12MS111 stationery rechargeable lead-acid batteries of 12V/95Ah in series-parallel association, resulting in a bank of 24V/190Ah per BSS. Therefore, the nanogrid's BSS model was adapted from the models developed by Machado et al. (2023). The SOC is maintained at 80% for the simulations.

The Battery Storage System, modeled with lead-acid batteries, is presented in Figure 6.

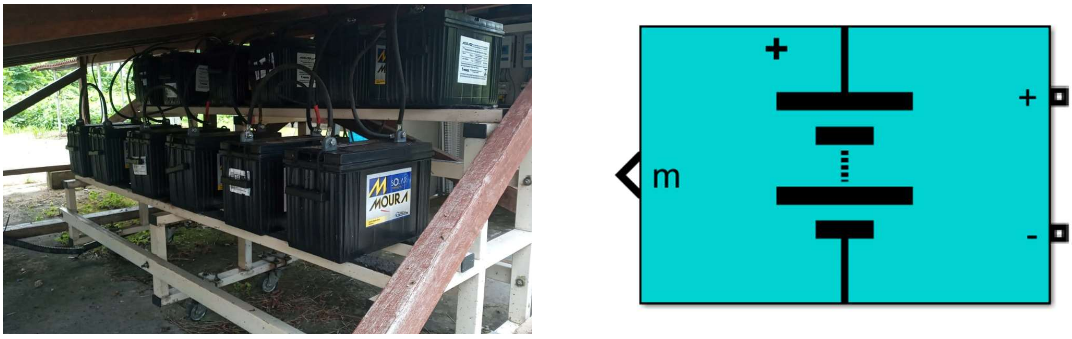

Figure 6: Battery storage system and their Simulink block.

2.4. Inverter

An off-grid inverter model in Simulink is adapted from the model developed by Tan, Chuin, et al. (2020). The off-grid inverter uses a 20 kHz high-frequency push-pull transformer inverter to step up the 24 V to 400 VAC and convert it back to DC through a full-bridge rectifier. The 400 V is then converted to 127 V in AC 60 Hz sinewave through H-bridge inverter with Sinusoidal Pulse Width Modulation and LC filter. The output voltage is controlled and maintained by PI feedback control. The off-grid inverter model is capable of converting 24 V from the distribution grid to 127 V 60 Hz up to a power rating of 1000 W. It achieved an average conversion efficiency of ≥ 94 % and produces a sinewave output waveform with a THD of less than 1 %. The performance of the Simulink model is also validated with the commercial off-grid inverter. The Simulink model presented can be flexibly changed to meet the commercial inverter with similar topology.

The off-grid inverter model used in the simulations is illustrated in Figure 7.

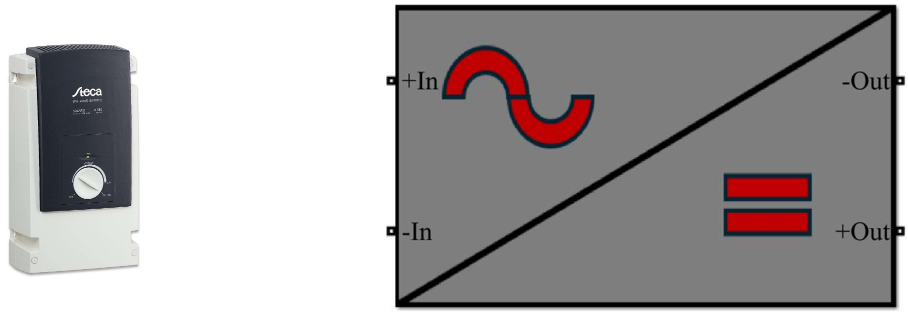

Figure 7: Inverter and its Simulink block.

2.5. Load Banks

Three load banks were selected to simulate a residential demand profile, considering buildings in a remote community in the Amazon served by DC distribution systems. Load Bank 1 (LB1) consists of a pure resistive load, designed for a nominal power demand of approximately 160–170 W. However, as a resistive load, its actual power dissipation depends on the voltage at its connection point. Load Bank 2 (LB2) is a resistive load with a 12 V voltage regulator, configured to operate as a constant power load of around 50 W.

Load Bank 3 (LB3) is composed of a load with an input stage consisting of a rectifier with a capacitive filter at the inverter's output. This configuration represents an AC electronic load composed of a 60 W television and combinations of lamps totaling around 24–30 W. The power demand of LB3 varies according to the load profile, ranging from 87 W to 360 W across Cases 1 to 5, allowing for dynamic simulation of AC load impacts on the DC grid.

2.6. Conductors

The distribution grid is formed by two conductors (+Vcc/ Vcc) type XLPE 0.6/1kV aluminium cable. According to the cable manufacturer ALUBAR there is an electric resistance of 0.837 Ω/km (Machado et al., 2023). Thus, the connections were modeled as resistors with a resistance calculated with this density.

Figure 8 provides the resistance values used in the grid modeling.

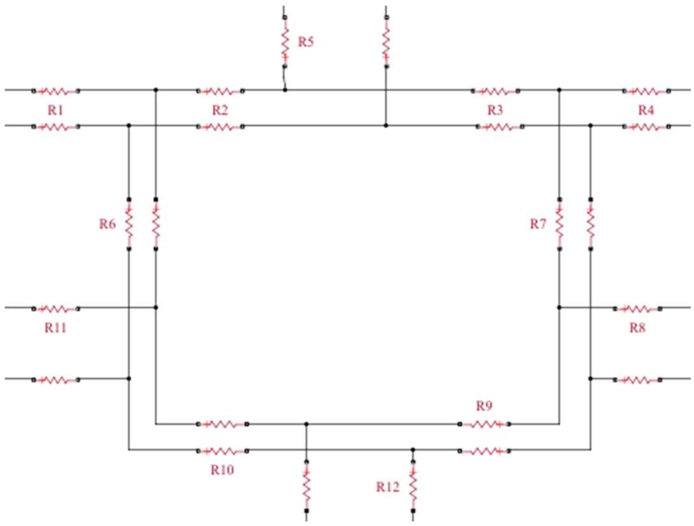

R_1 = 6.00 m	R_2 = 11.35 m	R_3 = 11.25 m	R_4 = 11.35 m	R_5 = 11.35 m	R_6 = 17.35 m
R_7 = 28.70 m	R_8 = 17.25 m	R_9 = 11.25 m	R_{10} = 38.35 m	R_{11} = 28.50 m	R_{12} = 9.65 m

Figure 8: DC distribution grid resistances.

3. Results and Discussion

Five simulations were conducted, each considering a different power demand scenario for LB3. All simulations were performed under an irradiance of 1000 W/m² and a cell operating temperature of 65 °C.

The simulations involved measuring electrical parameters—voltage and current—at the connection points of the load banks, observing that voltage ripple is directly related to current flow, particularly on the DC side that supplies the inverter. As the inverter demands more current on the AC side, the voltage ripple across the DC distribution grid increases. The fundamental frequency of the AC current reflected on the DC side is 120 Hz, which is twice the AC-side fundamental frequency.

Voltage and current ripples of varying magnitudes were identified at the DC distribution grid's load connection points in all simulations. Figure 9 shows the measurements at the connection points of LB1, LB2, and LB3 for the simulations. There are different ripple profiles, primarily due to the configuration of LB3, increasing the demand of the nonlinear load connected to the inverter output (AC side) and leading to more pronounced ripple distortions in the lower-demand cases.

Furthermore, the voltage at the connection points of LB1 and LB2 is influenced by the ripple introduced due to LB3, thus their magnitudes increase in response to the ripple in LB3. Notably, the ripple was more significant in LB2 than in LB1, due to the proximity of LB2 to LB3.

Figures 10 and 11 present the spectral components of the current and voltage at the load bank connection points, highlighting dominant peaks at 120 Hz. Other frequencies were also detected—60 Hz, 180 Hz, 240 Hz, and 360 Hz—with amplitudes exceeding 50 A at the LB3 connection point. These voltage and current spectral patterns are consistent with those found in experimental tests and reported by da Fonseca et al. (2025).

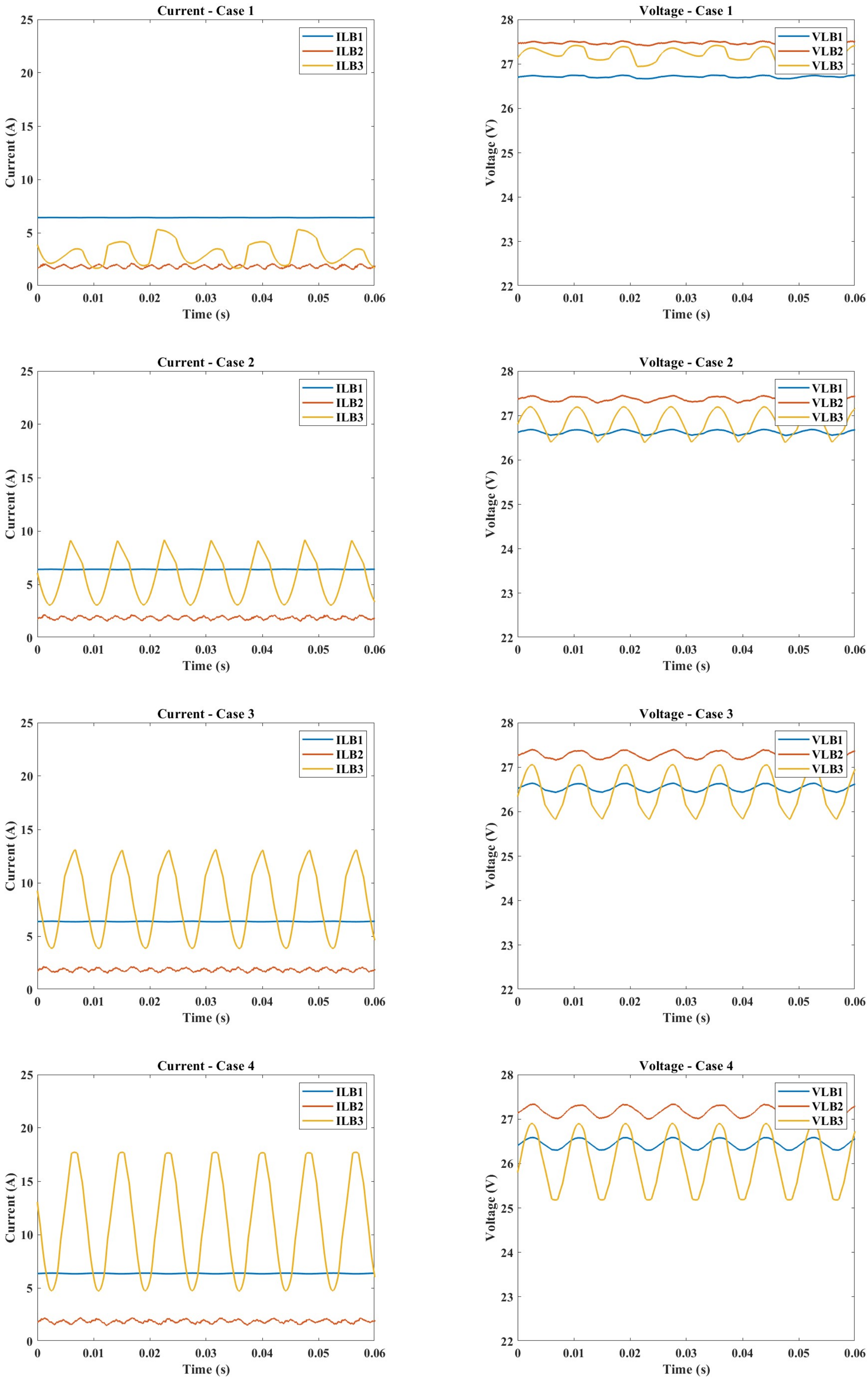
Current - Case 1
Voltage - Case 1
Current - Case 2
Voltage - Case 2
Current - Case 3
Voltage - Case 3
Current - Case 4
Voltage - Case 4
ILB1
ILB2
ILB3
VLB1
VLB2
VLB3
Current (A)
Voltage (V)
Time (s)

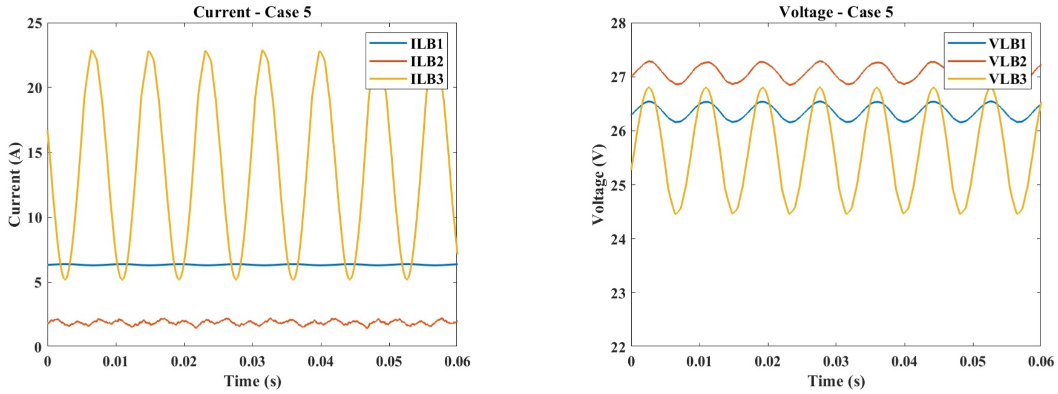

Figure 9: Current and voltage measurements at the load banks' connection points.

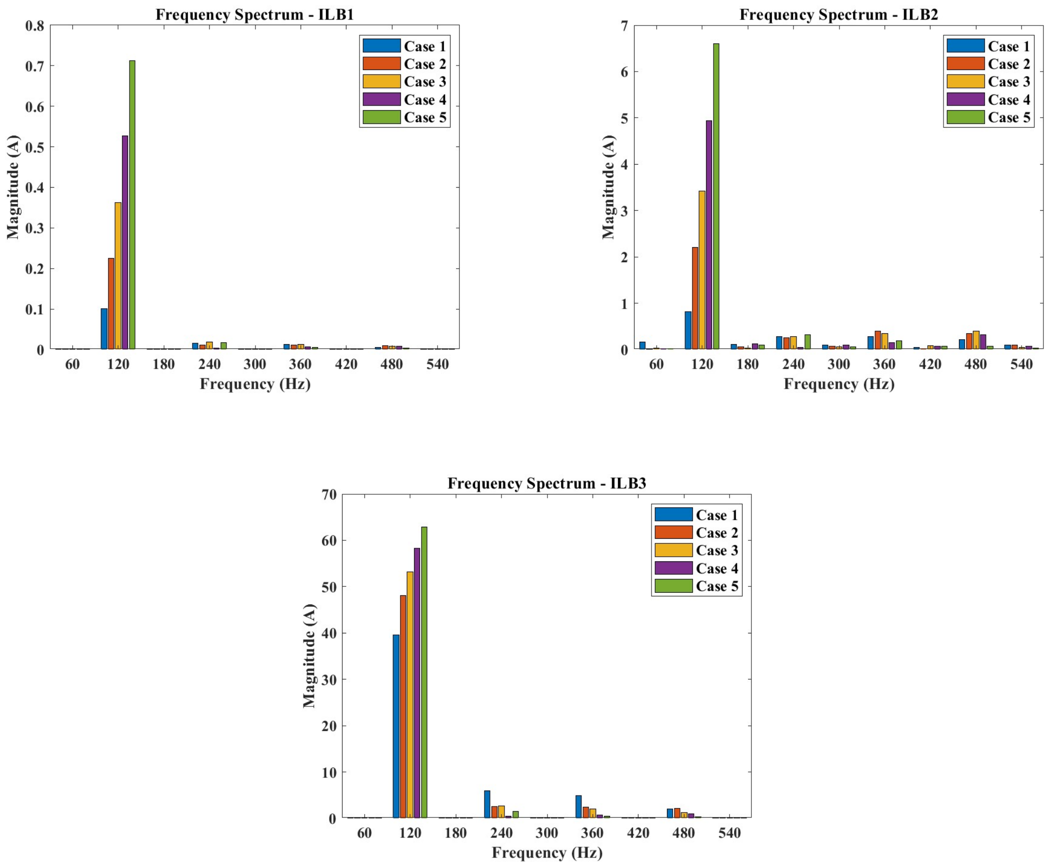

Figure 10: Harmonic spectrum of the current magnitude

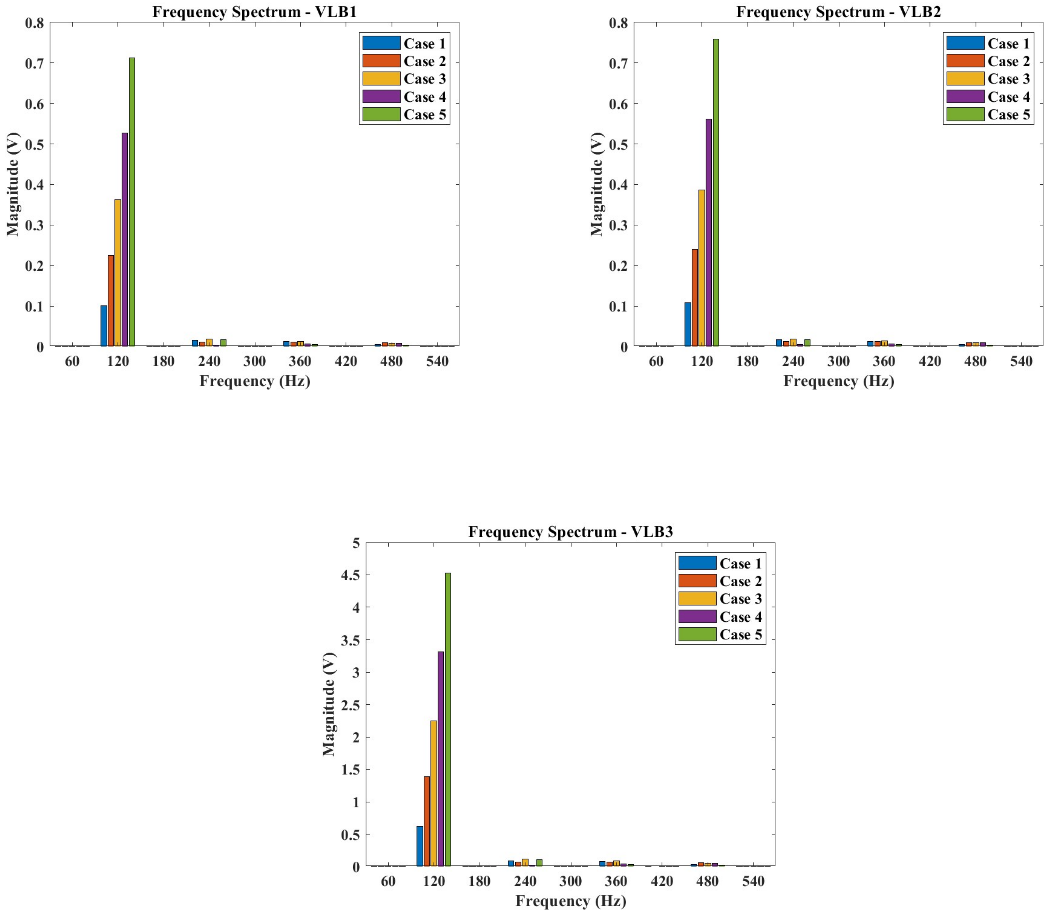

Figure 11: harmonic spectrum of the voltage magnitude

For evaluating voltage and current ripples, the indicators RMS ripple factor (*RF*) were utilized, aiming to assess the presence of AC component and its magnitude at different points in the distribution grid. Table 1 shows all cases of RMS ripple factor values for current and voltage for cases 1, 3, and 5. These cases were selected to represent a progressive increase in load demand, ranging from the lowest to the highest levels among the simulated scenarios.

The increase in voltage and current ripple at LB1 and LB2 points is influenced by the increase in voltage ripple magnitude at the LB3 connection point. Table 2 lists the values of apparent, active, and non-active power at the connection point of the LB3 loads. The simulation results showed a relationship between the *RF* and the non-active power demanded by LB3. Thus, the higher the *RF* values, the greater the non-active power demanded.

Below are the equations (eq. 1 and eq. 2) for calculating the Ripple Factor (*RF*) and the Non-Active Power (*Na*).

$$RF_x = \frac{\sqrt{\frac{1}{N}\sum_1^n (x_n - X_m)^2}}{X_m} x100\% \qquad \text{(eq. 1)}$$

- x_n, value at the n – measurement
- X_m, average value
- N, total of measurements at a period

$$Na = \sqrt{(V_{rms}I_{rms})^2 - P^2} \quad \text{(eq. 2)}$$

- V_{rms}, RMS value of the total voltage at the measurement point
- I_{rms}, RMS value of the total current at the measurement point
- P, active power

Tab. 1: *RF* for current and voltage calculated in cases 1, 3, and 5

%	Case 1			Case 3			Case 5		
	LB1	LB2	LB3	LB1	LB2	LB3	LB1	LB2	LB3
V - RF	0.08	0.09	0.52	0.26	0.28	1.60	0.50	0.53	3.21
I – RF	0.08	7.59	33.79	0.25	8.00	37.71	0.50	9.00	44.56

Tab. 2: Power measurement in LB3

Case 1			Case 3			Case 5		
VA	W	VAr	VA	W	VAr	VA	W	VAr
92.07	87.22	29.47	239.51	224.08	84.58	392.12	357.99	160.00

Finally, Table 3 shows the power losses in the distribution grid. The increase in the power demand by LB3 leads to higher power losses and greater losses associated with the circulation of AC components. Additionally, the PVG supplies 1.19 kW, and in the simulated scenarios, the losses represent a maximum of 3.62% of the available power.

Tab. 3: Power losses in distribution grid

Losses	Case I	Case II	Case III	Case IV	Case V
Total (W)	9.86	14.35	21.06	30.62	43.06
AC components (W)	0.15	0.53	1.35	2.82	5.11
%	1.57	3.69	6.41	9.22	11.87

These results show how steady-state operation of loads, such as inverters, can impact the distribution grid losses. Also, the insertion of AC components the distribution grid affects other loads. For example, the presence of AC components in the distribution grid impacts loads with a DC-DC converter, since an increase in nonactive power leads to a reduction in the power factor for these loads. Thus, Figure 12 shows the relation between the losses per section and the participation of harmonic components in the power losses. It can be noticed that in lower LB3 power demands, the power losses are strong in the connection point of LB1 (R_5), but as LB3's power demand increases, the power losses in the connection point of the LB3 (R_8) increase either.

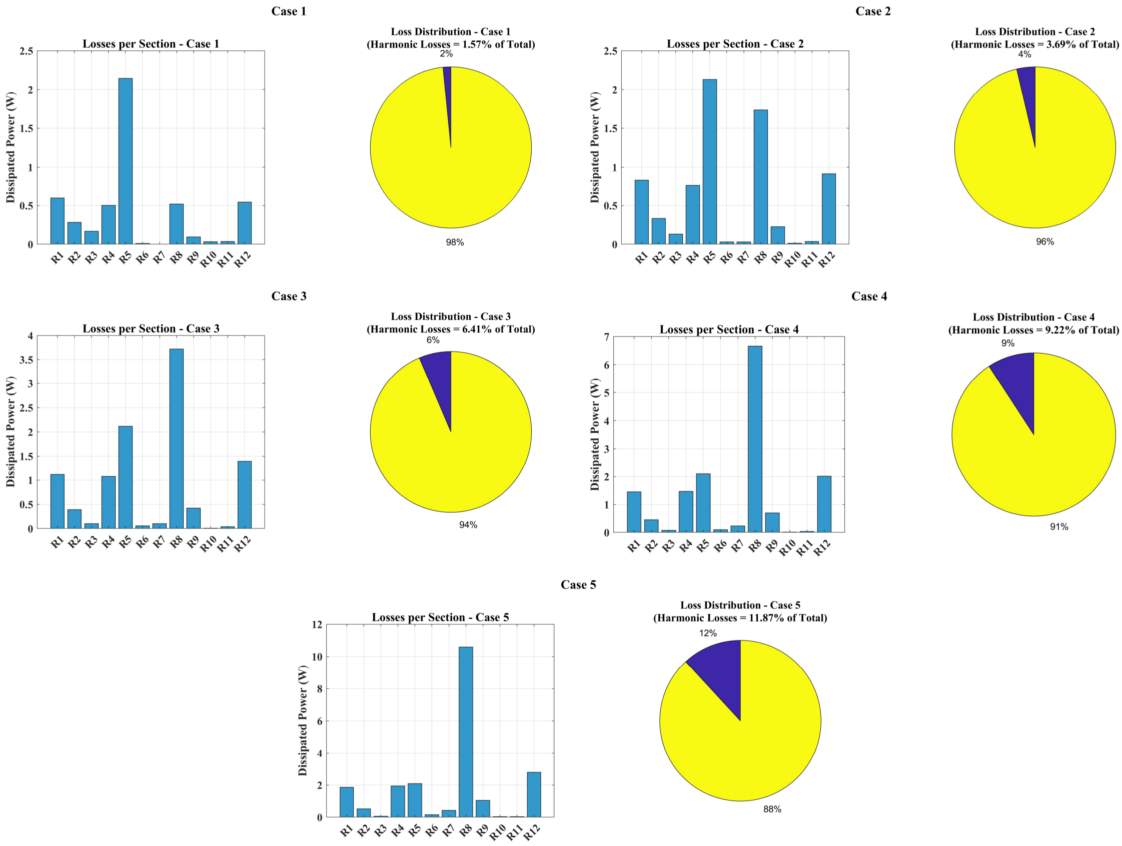

Figure 12: Losses per section and harmonic components losses.

4. Conclusion

This paper presented an analysis of current ripple in an open structure Direct Current Distribution Nanogrid (DCDN), based on a MATLAB/SIMULINK model of a real experimental system. The study focused on the impacts of an inverter operating under varying power demands on the DC grid's performance.

The simulation results demonstrated that the operation of the inverter is a primary source of current and voltage ripple within the DC nanogrid. A relationship was established between the AC load's power demand and the magnitude of the ripple, which propagates throughout the grid, affecting other connected loads. The fundamental frequency of this ripple on the DC side was 120 Hz, twice the fundamental frequency of the AC side, with other harmonic components also detected.

The simulations showed that as the RF values for voltage and current increase, so does the non-active power demanded by the inverter's load bank (LB3). Consequently, this leads to higher total power losses in the distribution grid at the moment analysed, which reached up to 11.87% of the available generated power in the highest demand scenario. This shows how AC components introduced by inverters can significantly compromise the overall efficiency of the DC system.

These preliminary impact assessments on the use of typical loads in DC nanogrids are important for the design, operational performance prediction, and implementation of more robust and efficient off-grid DC power systems, particularly in contexts like remote communities.

5. Acknowledgments

The authors would like to thank the support provided by National Council for Scientific and Technological Development - CNPq (Brazil): CNPq Processo: 408049/2022-7 - Chamada CNPq/MCTI 25/2022, CNPq Processos: 313432/2025-2 e 310679/2025-7 - Chamada CNPq 18/2024, and National Institute for Technological Development of Photovoltaic Solar Energy Applications, INCT-DAESF, CNPq/MCTI/Brazil, Process 408486/2024-4.

6. References

da Fonseca, A. C., Macêdo, W. N., & Galhardo, M. A. B., 2025. Impacts of power quality events on supplying loads in an experimental open structure DC nanogrid under different operating conditions. Electric Power Systems Research. 238, 111082. https://doi.org/10.1016/j.epsr.2024.111082

Fuchs, I., Rajasekharan, J., & Cali, Ü.,2024. Decentralization, decarbonization and digitalization in swarm electrification. Energy for Sustainable Development. 81, 101489. https://doi.org/10.1016/j.esd.2024.101489

Ma, Z., Li, Y., Sun, Y., & Sun, K., 2023. Low Voltage Direct Current Supply and Utilization System: Definition, Key Technologies and Development. CSEE Journal of Power and Energy Systems. https://doi.org/10.17775/CSEEJPES.2022.02130

Machado, J. P. de A., Reis, F. C., Côrrea, A. F., Bulhosa, L. D. S., Macêdo, W. N., & Galhardo, M. A. B., 2023. Simulation and Operational Evaluation of Distributed Storage Devices Connected to a Direct Current Distribuition Nanogrid. 2023 IEEE Latin American Electron Devices Conference (LAEDC). 1–5. https://doi.org/10.1109/LAEDC58183.2023.10209107

Tan, R. H. G., Chuin, C. B., & Solanki, S. G., 2020. Modeling of single phase off-grid inverter for small standalone system applications. International Journal of Power Electronics and Drive Systems (IJPEDS). 11(3), 1398. https://doi.org/10.11591/ijpeds.v11.i3.pp1398-1405

Tan, R. H. G., Er, C. K., & Solanki, S. G., 2020. Modeling of Photovoltaic MPPT Lead Acid Battery Charge Controller for Standalone System Applications. E3S Web of Conferences. 182, 03005. https://doi.org/10.1051/e3sconf/202018203005